

# A Fourier approach to fields and electron optical phase-shifts calculations

M. Beleggia<sup>a,\*</sup>, P.F. Fazzini<sup>b</sup>, G. Pozzi<sup>b</sup>

<sup>a</sup> *Materials Science Department, Brookhaven National Laboratory, Upton, NY 11973, USA*

<sup>b</sup> *Department of Physics and Istituto Nazionale per la Fisica della Materia, University of Bologna, Viale B. Pichat 6/2, 40127 Bologna, Italy*

Received 4 July 2002; received in revised form 12 November 2002

## Abstract

The Fourier method is applied to calculate fields and electron optical phase shifts in specimens having long-range electromagnetic fields, like reverse biased p–n junctions or stripe magnetic domains. It is shown that this approach not only allows to take into account rather easily the effect of the fringing fields protruding in the space around the specimen, but also to obtain solutions to interesting models in analytical form.

© 2002 Elsevier Science B.V. All rights reserved.

*PACS:* 61.14.–x; 73.40.Lq; 75.60.Ch

*Keywords:* Electron diffraction and elastic scattering theory; Image simulation

## 1. Introduction

Recently, by analysing the problem of the observation of superconducting fluxons by transmission electron microscopy, we have found that the calculation of the electron optical phase shift can be carried out successfully by a new analytical approach, where first the vector potential is decomposed into its Fourier components and then the phase shift is calculated for each component separately [1,2]. In this way the Fourier transform of the phase shift is immediately obtained, and can be inverted either analytically or numerically.

The main advantages of this approach are that the case of a periodic array of fluxons can be easily analysed, a troublesome problem in the former real space approach owing to the long-range behaviour of the fluxon magnetic field [1], and that new superconducting structures, like pancake vortices present in high- $T_c$  materials [3] or anisotropic fluxons, which were beyond the scope of the flux tube model and its implementations, can be successfully investigated [2,4].

In this work we have endeavoured to apply this approach also to other long range electromagnetic fields, in the belief that, even if the solution of the problem is known by real space methods, the Fourier approach can offer a useful different perspective or at least lead to computational benefits. First the case of reverse-biased p–n

\*Corresponding author. Tel.: +1-631-344-2110; fax: +1-631-344-4071.

*E-mail address:* [beleggia@bnl.gov](mailto:beleggia@bnl.gov) (M. Beleggia).

junction is considered. The theoretical analysis of this problem developed over the years [5–8] and finally has been thoroughly considered by Vanzi [9] who used Fourier methods in order to prove some important relations in real space. In particular, he also recognized that the phase shift of the external field can be Fourier inverted in order to re-obtain the potential over the specimen plane.

Here it will be shown how these results can be analyzed in the Fourier approach and how the comparison between real and reciprocal space can lead to a better understanding when numerical calculations by means of FFT are carried out, both for the one dimensional case, where the most significant terms of the phase shift are immediately recovered through the intervention of generalized functions, and for the two-dimensional case of a periodic array of p–n junctions in a semi-infinite specimen [10,11].

Finally, entering the domain of magnetism, a simple model describing alternate magnetic domains, again in a semi-infinite specimen, will be analysed, showing that the new approach not only allows us to obtain the Fourier transform of the phase shift, but that this latter can be inverted, leading to the analytical expression in real space [12]. Our results therefore complement and extend those obtained by Beardsley [13] and Mansuripur [14,15], who obtained the general relations in the Fourier space but subsequently specialized them under the assumption that the distribution of the magnetization is doubly periodic in order to apply Fast Fourier Transforms (FFT) methods for numerical calculation of the magnetic field, the vector potential and the phase shift.

## 2. General considerations

Let us consider the specimen in the form of a thin slab of constant thickness  $t$ , supporting charges and currents, i.e. the sources of electric and magnetic fields respectively, which may extend in the whole space. As customary in electron optics, see f.i. [16,17], the microscope coordinate system has the  $z$ -axis parallel to the electron beam and aligned in the same direction, whereas  $(x, y)$  are the coordinates in the object plane, perpendi-

cular to the optical axis. The origin of our coordinate systems is the intersection of the optical axis with the mid-plane of the specimen. By considering only elastic scattering events, the interaction of the specimen with the electron beam can be described through a complex transmission function (object wavefunction)  $O(x, y)$  which represents the ratio between the amplitudes of the out-going and the in-going electron wavefunctions.

In the standard phase-object approximation  $O(x, y)$  is given by

$$O(x, y) = a(x, y) \exp[i\varphi(x, y)], \quad (1)$$

where

$$\varphi(x, y) = \frac{\pi}{\lambda E} \int_{\ell} V(x, y, z) dz - \frac{2\pi e}{h} \int_{\ell} A_z(x, y, z) dz \quad (2)$$

and the amplitude term  $a(x, y)$  takes into account those electrons scattered at large angles and cut by the objective lens aperture. The integral is taken along a trajectory  $\ell$  parallel to the optical axis  $z$  inside and outside the specimen to include stray fields,  $V(x, y, z)$  and  $A_z(x, y, z)$  are the electrostatic potential and the  $z$  component of the magnetic vector potential  $\mathbf{A}(x, y, z)$ , respectively.  $E$  is a parameter dependent on the accelerating voltage (and equal to it in the non-relativistic approximation) having the dimension of an electrostatic potential [18], and  $e$ ,  $\lambda$ ,  $h$  are the absolute value of the electron charge, the electron wavelength and the Planck constant, respectively.

The specimen divides the space into three regions: I for  $z \geq t/2$ , II for  $|z| < t/2$  and III for  $z \leq -t/2$ . Therefore Eq. (2) can be formally split into three contributions

$$\varphi = \varphi^I + \varphi^{II} + \varphi^{III}. \quad (3)$$

It is worthwhile to emphasize that, although it may be convenient to speak of internal and external fields and phase shifts, the physical observable is the sum of the three contributions, not each of them separately. It is also important to recall that, contrary to the optical case where three-dimensional effects are strikingly impressive, only essentially two-dimensional information is

available in transmission electron microscopy. In fact in the electric case  $\varphi$  is proportional to the potential integrated along the electron path whereas, in the magnetic case, the maximum of information encoded in the beam corresponds to the magnetic flux enclosed between two trajectories.

In the vacuum regions surrounding the specimen, the electrostatic potential (as well as the  $z$ -component of the magnetic vector potential [1,2]) satisfies the Laplace equation

$$\nabla^2 V(x, y, z) = 0. \quad (4)$$

Let us consider region I. It can be easily ascertained that the general solution of the Laplace equation well behaved at infinity can be written as

$$V^I(x, y, z) = \frac{1}{4\pi^2} \int \int dk_x dk_y \tilde{V}(k_x, k_y, t/2) \times e^{ik_x x} e^{ik_y y} e^{-k_\perp(z-t/2)}, \quad z \geq t/2, \quad (5)$$

where  $k_\perp = \sqrt{k_x^2 + k_y^2}$ . The Fourier transform  $\tilde{V}(k_x, k_y, t/2)$  refers to the potential distribution at the specimen surface  $z = t/2$  and is given by

$$\begin{aligned} & \tilde{V}(k_x, k_y, t/2) \\ &= \int \int dx dy V^I(x, y, t/2) e^{-ik_x x} e^{-ik_y y} \end{aligned} \quad (6)$$

From expression (5) it is immediately ascertained that, integrating along  $z$ , the corresponding contribution to the phase shift is given by

$$\begin{aligned} \varphi^I(x, y) &= \frac{\pi}{\lambda E} \frac{1}{4\pi^2} \int \int dk_x dk_y \frac{\tilde{V}(k_x, k_y, t/2)}{k_\perp} \\ &\times e^{ik_x x} e^{ik_y y}. \end{aligned} \quad (7)$$

This equation allows us to extract the simple and significative relation in the Fourier space:

$$\tilde{\varphi}^I(k_x, k_y) = \frac{\pi}{\lambda E} \frac{\tilde{V}(k_x, k_y, t/2)}{k_\perp}. \quad (8)$$

These considerations can be extended also to region III, leading to

$$\tilde{\varphi}^{III}(x, y) = \frac{\pi}{\lambda E} \frac{\tilde{V}(k_x, k_y, -t/2)}{k_\perp} \quad (9)$$

highlighting the fact that the calculation of the external phase shift in the Fourier space, at least formally, is a very simple matter, once the

potential distribution on the two surfaces of the specimen is known. Vice versa, provided the potential at the upper and lower surfaces are equal and the contribution of the internal field is negligible, the surface potential distribution can be recovered at least formally from the phase shift by the inverse operation [9].

### 3. One-dimensional reverse-biased p-n junction

The aim of this section is to reconsider, within the realm of the Fourier space approach, the models developed for the interpretation of Lorentz images of one-dimensional reverse-biased p-n junctions, i.e. a straight junction in an infinite specimen of constant thickness  $t$ , lying along the  $y$ -axis, with an internal potential distribution depending only on the  $x$  coordinate.

Let us recall that all the relevant calculations can be carried out analytically in the real space [5,6,9], and that the simplest model is the Spivak one [19], where the potential distribution within the specimen and on the specimen surfaces is described by

$$V^II(x) = \frac{V_R}{\pi} \arctan\left(\frac{x}{d}\right), \quad (10)$$

where  $V_R$  is the reverse potential drop across the junction and  $d$  plays the role of the depletion layer half-width. The abrupt step model is obtained in the limit  $d \rightarrow 0$ .

The potential distribution in the external space  $z > t/2$  is given by

$$V^I(x, z) = \frac{V_R}{\pi} \arctan\left(\frac{x}{z + d - t/2}\right) \quad z > t/2 \quad (11)$$

with a similar expression for  $z < t/2$ . However, when the phase shift is calculated according to Eq. (2), a divergent result is obtained, depending on the fact that, according to Eq. (11), the external field extends significantly to infinity. In order to obtain a non-divergent result it is necessary to introduce either a cut-off distance [5], or boundary conditions stating the finiteness of the potential distribution [6,9]. In both cases these conditions lead to the introduction of linear terms in the phase, which can be safely neglected for the

interpretation of Lorentz images as they correspond to a rigid lateral translation of the diffraction pattern.

Let us show how these results can be viewed from the perspective of the Fourier approach. The Fourier transform of the potential (10) at the specimen surface  $z = t/2$  is given by

$$\tilde{V}(k_x, k_y, t/2) = V_R e^{-d|k_x|} \frac{2\pi\delta(k_y)}{ik_x}, \quad (12)$$

where  $\delta$  is the Dirac- $\delta$  distribution [20–24], so that, using Eq. (5) the potential in region I, after integrating over  $k_y$ , is given by

$$V^I(x, z) = \frac{1}{2\pi} \int dk_x \frac{V_R}{ik_x} e^{-d|k_x|} e^{-|k_x|(z-t/2)} \times e^{ik_x x}, \quad z > t/2 \quad (13)$$

a transform which can be inverted, recovering Eq. (11).

According to Eq. (7), we obtain immediately for the Fourier transform of the phase shift

$$\tilde{\varphi}^I(k_x, k_y) = -\frac{iV_R e^{-d|k_x|}}{\lambda E} \frac{\pi\delta(k_y)}{k_x k_\perp}. \quad (14)$$

Also the inverse Fourier transform of this expression can be obtained, within the realm of distribution theory [20–24]. However, different results are present in the literature, although referred to the parent case of the step function: according to Lighthill [21] and Jones [22] the inverse transform is given by the following generalized function:

$$\varphi^I(x) = -\frac{V_R}{\lambda E} x \log(x^2 + d^2) + \frac{V_R}{\lambda E} Cx, \quad (15)$$

where  $C$  is an arbitrary constant, whereas according to Richards and Youn [23] it is given by

$$\varphi^I(x) = -\frac{V_R}{\lambda E} x \log(x^2 + d^2) + \frac{V_R}{\lambda E} [x(1 - \gamma)], \quad (16)$$

where  $\gamma \simeq 0.577$  is the Euler-gamma constant. It can be noted that, in spite of the unessential difference in the linear term, both expressions give the same significant term in the phase [9] and that the divergence of the phase present in the real space approach is not present in the framework of the generalized functions. It is worthwhile to give an example which shows that the external field contribution is not negligible. Assuming a

specimen thickness of 200 nm, a potential difference of 1 V, a depletion region width of 100 nm and an accelerating voltage of 300 kV, the resulting maximum external phase difference, calculated from Eq. (16), is around 12 rad. The maximum internal phase difference, which is proportional to the potential, is instead around 0.5 rad, giving a ratio of  $\frac{1}{24}$  between the two contributions. In other cases, for example for thicker specimens, this ratio may vary considerably. However, the external contribution, in terms of maximum phase difference, is often predominant.

It is instructive to consider the problem of the numerical inversion of the Fourier transform, because very often it is not possible to perform the analytical one. Therefore, the numerical analysis of the foregoing model, where both approaches are possible, can give useful hints of the peculiar problems related to this issue. As explained pictorially in a very effective way in the books of Brigham [25] and Bracewell [26], the finite discretization and periodization introduces some errors, linked to the Gibbs [27] and aliasing phenomena [25,26], which should be kept under control in order to obtain reliable results.

Let us focus our attention on the more cumbersome external field, by considering, for simplicity, the case of the step model, which, as previously stated, can be obtained from the Spivak one when  $d \rightarrow 0$ . As the numerical inversion is usually carried out by using Fast Fourier Transform (FFT) algorithms, we need to sample the function in the Fourier space over a discrete and finite set of points, containing the origin at their center. If  $1/L$  is the spacing in the reciprocal space and  $N$  the pixel number, the inverted phase in the real space has a periodicity of  $L$  and vanishes at both the extremes of this interval, as shown in Fig. 1, where the phase is reported in arbitrary units, for  $L = 10 \mu\text{m}$  and  $N = 512$ , as a continuous line plot.

In order to compare this result with the analytical one, it is necessary to subtract a linear term over the same interval  $L$  in such a way that this linearized phase vanishes at the interval extremes. Let us recall that this linearization is also necessary for the numerical calculation of out-of-focus patterns in order to avoid the strong diffraction effects arising at the edges of the finite

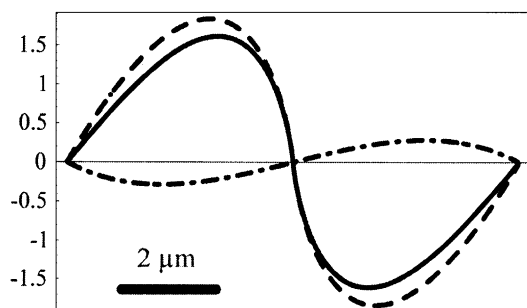


Fig. 1. Comparison between the phase shift of an abrupt junction calculated by means of the FFT algorithm (continuous line) and from the analytical expression (dashed line). The difference between the two (point-dashed line) is also reported.

interval. The obtained result, shown as a dashed plot line in Fig. 1 is rather similar, but not identical to the previous one, as better demonstrated by the difference between the two (point-dashed curve in Fig. 1). Clearly this difference is not negligible, compare f.i. the ordinate ranges, but is linear across the origin, where the step junction is located.

By changing  $L$  and  $N$ , patterns of almost identical shape are obtained, although abscissa and ordinate ranges are obviously different, in agreement with the fact that the step model has no characteristic length. This means that both procedures give intrinsically different results and the origin of this discrepancy depends on the fact that they are not able to cope with the boundary conditions of the initial model, stating that the potential does not vanish at infinity. The discretization processes correspond to models having different and strictly speaking rather unphysical periodic boundary conditions.

While this fact points out that the overall phase depends on the boundary conditions, so that f.i. in holography experiments they should be correctly taken into account, as far as regards out-of-focus images, both approaches give comparable results for the phase and image contrast across the junction, provided the width of the linear region is sufficiently larger than the dimension of the Fresnel zone. However, the choice of the interval  $L$  and the pixel number  $N$  plays here a more critical role than in the fluxon case [2].

#### 4. Parallel array of abrupt p–n junctions in a half-plane

Recently, an analytical model for the electric field associated to a periodic array of alternating p- and n-doped stripes lying in a half-plane, tilted with respect to the specimen edges, has been developed. As the specimen thickness has been neglected, the problem is equivalent to that of finding the electrostatic potential  $V(x, y, z)$  produced by a parallel array of stripes having width  $b$  (and pitch in the  $y$  direction  $b/\cos \alpha$ ) which lie in the positive half-plane ( $z = 0; x \geq 0$ ), tilted at an angle  $\alpha$  with respect to the edge normal ( $-\pi/2 < \alpha < \pi/2$ ) [10,11]. The stripes are biased at alternate potential, namely  $-V_R/2$  for p-doped and  $V_R/2$  for n-doped stripes, so that this model corresponds to an array of abrupt step junctions, as sketched in Fig. 2.

The problem was complicated because we did not know the potential over the whole plane  $z = 0$ , but only on the half-plane, so that in order to solve it correctly we exploited the striking similarity with the well-known optical problem of the diffraction of an inclined plane wave by a perfectly conducting half-plane [28–30].

The main results of our previous analysis [11] are briefly recalled in the following. On the specimen half-plane ( $z = 0, \geq 0$ ), the potential can be written as a Fourier series

$$V_\alpha(x, y) = \sum_{n=-\infty}^{+\infty} \gamma_n \exp \left[ \frac{i\pi n}{b} (y \cos \alpha + x \sin \alpha) \right], \quad (17)$$

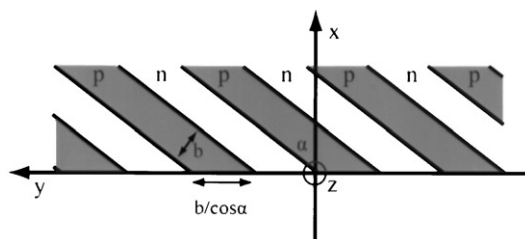


Fig. 2. Coordinate system and set-up of the alternatively p and n-doped regions in a semi-infinite specimen. Each stripe, of width  $b$ , is tilted at an angle  $\alpha$  with respect to the  $x$ -axis in the  $(x, y)$  plane.

where the coefficients  $\gamma_n$  are given, for the step junction model, by

$$\gamma_n = \frac{iV_R}{2\pi n} [(-1)^n - 1] = \begin{cases} -\frac{iV_R}{n\pi} & \text{for } n \text{ odd,} \\ 0 & \text{for } n \text{ even.} \end{cases} \quad (18)$$

By introducing new variables  $(p_n, q_n)$ , defined as

$$\begin{aligned} p_n &= \frac{\pi n}{b} \cos \alpha \\ q_n &= \frac{\pi n}{b} \sin \alpha \end{aligned} \rightarrow k_n = \sqrt{p_n^2 + q_n^2} = \left| \frac{\pi n}{b} \right| \quad (19)$$

in order to keep the notation compact, it turns out that the solution of the Laplace equation over the whole space is given by

$$V(x, y, z) = \sum_{n=-\infty}^{+\infty} \gamma_n V_n(x, z) e^{i(xq_n + yp_n)}, \quad (20)$$

where the coefficients  $V_n(x, z)$  can be written as

$$V_n(x, z) = \int_0^\infty p(\xi) V_{el}(x - \xi, z) d\xi \quad (21)$$

with

$$p(\xi) = C_n e^{i\xi q_n} \quad (22)$$

$C_n$  being

$$C_n = k_n \frac{\sqrt{\cos \alpha}}{\sqrt{\pi}} \exp\left[-i\frac{\alpha}{2} S(n)\right] \quad (23)$$

where  $S(n)$  is the Sign function. Finally, in polar coordinates ( $x = \rho \cos \theta$ ;  $z = \rho \sin \theta$ ),  $V_{el}$  is given by [11]

$$V_{el}(\rho, \theta) = \frac{e^{-\rho|p_n|}}{\sqrt{\rho|p_n|}} \sin \frac{\theta}{2} \quad (24)$$

If the potential distribution is written in the  $z = 0$  plane, by introducing the Heaviside step function  $H(\xi)$ , defined as

$$H(\xi) = \begin{cases} 1 & \xi > 0, \\ 0 & \xi < 0, \end{cases} \quad (25)$$

it results

$$V_n(x, 0) = \int_{-\infty}^{\infty} p(\xi) H(\xi) V_{el}(x - \xi, 0) d\xi \quad (26)$$

whose form suggests that its appearance should be simpler in the Fourier space, where convolution is changed into multiplication.

In fact, it can be ascertained that the Fourier transform of  $V_{el}(x, 0)$  is given by

$$\tilde{V}_{el}(k_x, 0) = \sqrt{\frac{\pi}{|p_n|(|p_n| - ik_x)}} \quad (27)$$

whereas that of  $p(x)H(x)$  is

$$C_n \left[ \pi \delta(k_x - q_n) - \frac{i}{k_x - q_n} \right], \quad (28)$$

so that, taking into account the properties of the Dirac- $\delta$  distribution, it results for the FT of  $V_n(x, 0)$

$$\tilde{V}_n(k_x, 0) = \pi \delta(k_x - q_n) - \frac{i}{k_x - q_n} \sqrt{\frac{|p_n| - iq_n}{|p_n| - ik_x}} \quad (29)$$

since, using (19)  $C_n$  can also be written as

$$C_n = \frac{\sqrt{|p_n|}}{\sqrt{\pi}} \sqrt{|p_n| - iq_n} \quad (30)$$

It can be verified after some cumbersome calculations that the above expression is actually the Fourier Transform of the expression found in our previous work [11]. While this analytical check confirms the soundness of our considerations, it can also be useful in order to compare the performance of the numerical FT inversion against the analytical expression. Fig. 3(a) reports the typical trend of the Fourier component of the electrostatic potential  $V_n(x, 0)$ . It can be seen that the function has value 1 for  $x > 0$  as expected on the basis of the boundary conditions, but it is also different from zero in the region  $x < 0$ , where it decreases to this value in a roughly exponential way, dictated by the value of  $q_n$ .

If we subtract the unit-step contribution in the positive  $x$  region, it turns out that the remaining term, shown in Fig. 3(b), is well behaved at infinity and hence should have a non-singular transform. Therefore, when we are facing the problem of the numerical inversion of Eq. (29) we can dispose of the singularity at  $k_x = q_n$  by adding and subtracting

$$\frac{-i}{(k_x - q_n)}. \quad (31)$$

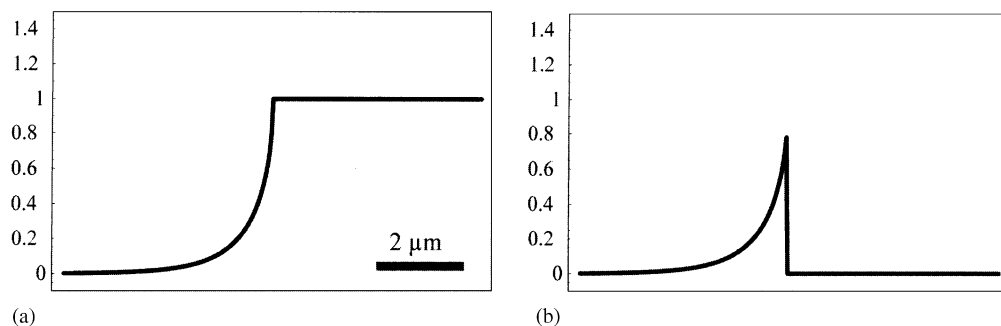


Fig. 3. Trend of the absolute value of the Fourier component of the electrostatic potential (a); the same but with the unit step subtracted (b).

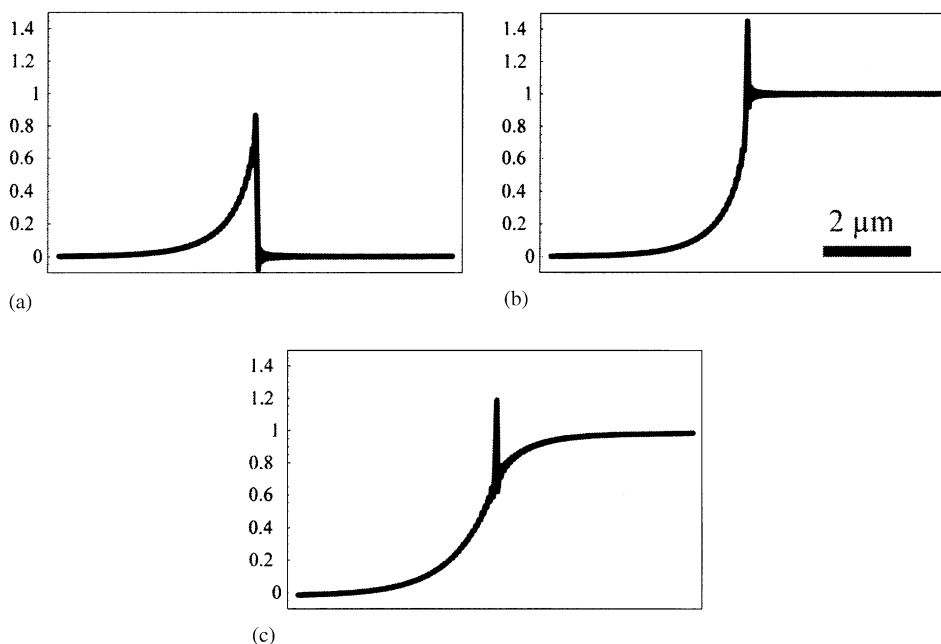


Fig. 4. Mixed numerical-analytical method: electrostatic potential before (a) and after (b) adding the unit step function; (c) same technique applied for the phase shift.

This term, combined with the Dirac *delta*-function of Eq. (29), gives a unit step function when inverted, whereas its opposite, combined with the second term of Eq. (29) gives a result that is no longer singular at the origin and its numerical inversion does not present troubles linked to the distribution behaviour. The result of this procedure is shown in Fig. 4(a), whereas 4(b) shows the trend of the function when the unit-step is summed. It can be noted that strong oscillations

are present in correspondence with the abrupt edge, and this effect is a manifestation of the Gibbs phenomenon [27], linked to the finite truncation of an otherwise infinite series. Several smoothing procedures can be employed in order to circumvent it [27], although, in the discontinuous case, still some errors are present at the edge between analytical and numerical expressions.

The usefulness of the Fourier approach is better evident when the phase shift is calculated, because

in this case the time-consuming integration along  $z$  of the potential (whose expression in the whole space is much more complicated with respect to its value on the plane  $z = 0$  [11]) is replaced by the multiplication of the FT of the potential, Eq. (29), by the factor

$$\frac{\pi}{\lambda E k_{\perp}} \quad (32)$$

By using the same stratagem of mixed analytical numerical inversion on the resulting expression for the Fourier transform of the  $n$ -coefficient, the result shown in Fig. 4(c) is obtained, showing that the function slowly decreases from a constant value for large positive values of  $x$  to zero for large negative ones, with still the Gibbs phenomenon present in correspondence of the edge.

When these findings are put together to calculate the phase shift due to the external field, we obtain the results shown in Fig. 5, where the phase shift is calculated by the Fourier methods (a) and by numerical integration in the real space (b). It can be ascertained that the agreement between the two methods is satisfying, apart from the edge region owing to the detrimental effect of the Gibbs phenomenon. However the Fourier based algorithm is much less time consuming. For instance, the calculation in real space needs about 2 h on a standard Desktop computer (Power Macintosh G3) with respect to 10 min for the calculation in Fourier space, performed with the same hardware.

## 5. Stripe magnetic domains in a half-plane

Following the same formalism employed in developing the p–n junction models, we can extend the results to the magnetic case. The basic difference between electrostatic and magnetic cases, is that we have to deal with a vector potential rather than the scalar electrostatic potential. The phase shift, as shown in Eq. (2), can be calculated as a line integral along the optical axis of the  $z$ -component of the vector potential  $\mathbf{A}$ .

The general expression linking magnetization and vector potential

$$\mathbf{A}(\mathbf{r}) = \frac{\mu_0}{4\pi} \int \mathbf{M}(\mathbf{r}') \times \frac{\mathbf{r} - \mathbf{r}'}{|\mathbf{r} - \mathbf{r}'|^3} d^3\mathbf{r}' \quad (33)$$

which can be found in any electromagnetism book (see f.i. [15]) represents the starting point for calculating the vector potential starting from a known magnetization configuration. Eq. (33) can be written in Fourier Space, exploiting the convolution theorem and the linearity of the cross product, as

$$\tilde{\mathbf{A}} = \frac{\mu_0}{4\pi} \tilde{\mathbf{M}} \times \mathcal{F} \left[ \frac{\mathbf{r}}{r^3} \right]. \quad (34)$$

Therefore we can apply the formalism introduced in the previous sections, and develop a Fourier space approach to calculate the phase shift for interesting configurations. The three-dimensional Fourier transform of the function  $\mathbf{r}/r^3$

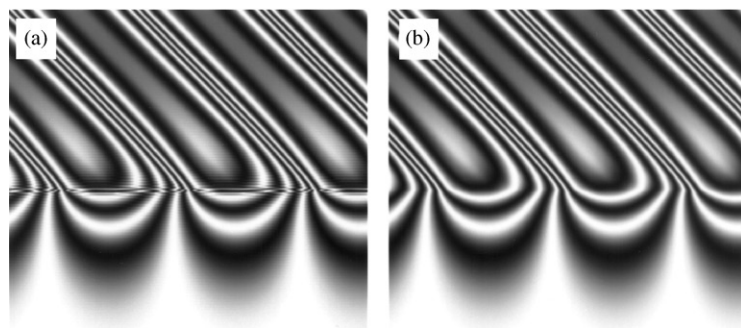


Fig. 5. Phase shift of an array of p–n junction tilted at  $\alpha = 45^\circ$  displayed as a holographic contour map. (a) Result of the Fourier method; (b) direct integration in real space.

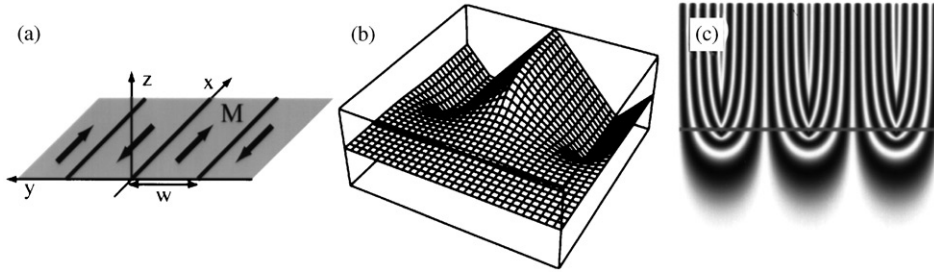


Fig. 6. (a) Magnetic configuration of the specimen: a semi-infinite array of  $180^\circ$  stripe domains. The specimen edge is coincident with the  $y$ -axis of the reference system. Phase shift of three stripe domains displayed as a three-dimensional plot (b) and as a holographic contour map (c) where the grey line corresponds to the specimen edge.

which is present in Eq. (33) can be calculated in cartesian coordinates, integrating with respect to each variable independently, and the result turns out to be

$$\mathcal{F}\left[\frac{\mathbf{r}}{r^3}\right] = -4i\pi \frac{\mathbf{k}}{k^2}. \quad (35)$$

Therefore, once the magnetization is given, the vector potential and the electron optical phase shift can be calculated in the Fourier space approach.

Let us now consider a thin specimen of thickness  $t$ , lying on the  $(x, y)$  plane and containing an array of  $180^\circ$  magnetic domains of width  $w$  each alternatively oriented along the positive or negative direction on the  $x$ -axis. The specimen is considered semi-infinite, which means that there is an abrupt termination along the  $y$ -axis at  $x=0$ . The setup is sketched in Fig. 6(a).

The magnetization can be expressed as

$$\mathbf{M} = \frac{N\phi_0}{\mu_0 t w} [1, 0, 0] H(x) Q(y) U(z), \quad (36)$$

where  $\phi_0$  is the flux quantum  $h/2e$ , and  $N$  is the number of flux quanta trapped inside the domain (not necessarily an integer number, as the flux quantization does not apply here). The function  $Q(y)$ , representing a square wave of width  $w$ , is given by

$$Q_w(y) = \begin{cases} 1 & (2n)w \leq y < (2n+1)w \\ -1 & (2n+1)w \leq y < (2n+2)w \end{cases} \quad (37)$$

for  $n = 0, \pm 1, \dots$

and the function  $U(z)$ , describing the specimen thickness, is defined as

$$U(z) = \begin{cases} 1 & |z| < t/2, \\ 0 & |z| > t/2. \end{cases} \quad (38)$$

As the three functions in Eq. (36),  $H(x)$ ,  $Q(y)$ ,  $U(z)$  depend on different variables, we can express the Fourier transform of the magnetization as the product of the transforms of these functions, namely

$$\tilde{H}(k_x) = \pi \delta(k_x) + \frac{1}{ik_x}, \quad (39)$$

$$\tilde{Q}_w(k_y) = \frac{i\pi}{wk_y} (1 - e^{-iwk_y})^2 \sum_{n=-\infty}^{+\infty} \delta\left(k_y + \frac{\pi n}{w}\right) \quad (40)$$

which, considering the properties of the Dirac- $\delta$  distribution may be also written as

$$\tilde{Q}_w(k_y) = \frac{4\pi i}{wk_y} \sum_n^{\text{odd}} \delta\left(k_y + \frac{\pi n}{w}\right). \quad (41)$$

Finally

$$\tilde{U}(k_z) = \frac{2}{k_z} \sin\left(\frac{k_z t}{2}\right) \quad (42)$$

so that the Fourier transform of the  $\mathbf{M}$  vector is

$$\tilde{\mathbf{M}} = \frac{N\phi_0}{\mu_0 w t} [1, 0, 0] \tilde{H}(k_x) \tilde{Q}(k_y) \tilde{U}(k_z). \quad (43)$$

Considering the result found in Eq. (35), thus performing the cross product between  $[1, 0, 0]$  and  $\mathbf{k} = [k_x, k_y, k_z]$ , we can directly write the expression

for the vector potential

$$\tilde{\mathbf{A}} = 8\pi \frac{N\phi_0}{w^2 t} \frac{[0, -k_z, k_y]}{k_y k_z k^2} \left[ \pi \delta(k_x) + \frac{1}{ik_x} \right] \times \sum_n^{\text{odd}} \delta\left(k_y + \frac{\pi n}{w}\right) \sin\left(\frac{ik_z}{2}\right). \quad (44)$$

Extracting the  $z$ -component of the vector potential, performing the integration along the  $z$ -axis and going back to real space, we obtain the phase shift, in analytical but implicit form:

$$\varphi(x, y) = -\frac{4N}{w^2} \int dk_y e^{iyk_y} \sum_n^{\text{odd}} \delta\left(k_y + \frac{\pi n}{w}\right) \times \int dk_x \left[ \pi \delta(k_x) + \frac{1}{ik_x} \right] \frac{e^{ixk_x}}{k_x^2}. \quad (45)$$

This phase shift can be put into a Fourier-series expansion, and finally summed in order to have it in closed form by the following steps. First, we perform the integration on  $k_x$  obtaining

$$\int dk_x \left[ \pi \delta(k_x) + \frac{1}{ik_x} \right] \frac{e^{ixk_x}}{k_x^2} = \frac{i\pi}{k_y^2} [2H(x) - S(x)e^{-|xk_x|}] \quad (46)$$

then, exploiting once again the properties of the Dirac- $\delta$  distribution, we obtain the Fourier-series expression

$$\varphi(x, y) = \frac{N}{2\pi} \sum_{n=0}^{+\infty} \frac{\cos[(2n+1)\pi y/w]}{(n+1/2)^2} \times [2H(x) - S(x)e^{-n\pi|x|/w}]. \quad (47)$$

Considering that the cosine is the real part of the complex exponential, the phase shift can be also written more conveniently as

$$\varphi(x, y) = \frac{N}{2\pi} \operatorname{Re} \left( e^{i\pi y/w} \sum_{n=0}^{+\infty} \frac{e^{2ni\pi y/w}}{(n+1/2)^2} \times [2H(x) - S(x)e^{-n\pi|x|/w}] \right). \quad (48)$$

Now, recalling the definition of the generalized  $\Phi$  function (i.e. a generalization of the Riemann Zeta and Polylogarithmic functions), also called

Lerch function [31], given by

$$\Phi_v^s(z) = \sum_{n=0}^{+\infty} \frac{z^n}{(n+v)^s}, \quad (49)$$

where it is assumed that any term with  $n+v=0$  is excluded, and considering the values  $s=2$ ,  $v=\frac{1}{2}$ , we can sum the Fourier-Series, and obtain the final result in analytical form as

$$\varphi(x, y) = \frac{N}{2\pi} \operatorname{Re} [2H(x)e^{\pi(iy/w)} \Phi_{1/2}^2(e^{2\pi(iy/w)}) - S(x)e^{\pi(iy-|x|)/w} \Phi_{1/2}^2(e^{2\pi(iy-|x|)/w})]. \quad (50)$$

The phase shift (in arbitrary units) corresponding to a region enclosing three domains is reported in Fig. 6(b). The simulated holographic fringes, Fig. 6(c), are curved near the specimen edge, indicating a strong demagnetizing effect. Moreover, inside the specimen (for  $x > 0$ ) the fringes form a sharp angle, while in the vacuum they connect more smoothly. This effect is mainly due to the zero-width model assumed for the domain walls.

## 6. Conclusions

In this work we have tried to show how the Fourier approach can be a very powerful tool for the calculation of long range electromagnetic fields and corresponding electron optical phase shifts.

In particular we have shown how in the one-dimensional p–n junction case it has been possible to immediately recover the most significative terms of the electron optical phase-shift. Moreover, the discrepancies arising in the comparison between numerical results obtained by the two approaches (real and Fourier) point out the relevance of the boundary conditions and the critical role played by the choice of the interval and pixel number. For the two-dimensional p–n junction case we have shown that the Fourier transform of the phase can be obtained in a rather simple analytical form, and this is leading to a gain of an order of magnitude in computing time when numerical calculation of the phase is necessary. Finally, we have shown that the Fourier approach allows us to obtain the analytical solution to the phase shift of an array of magnetic stripe domains lying in a half-plane.

We have focused our attention on the half-plane geometry, because this set-up is the most frequent in electron holography experiments, where usually the reference wave is taken from the vacuum region and may be therefore perturbed by the fringing field protruding from the specimen edge. The numerical approach with its doubly periodic boundary conditions is in fact unable to cope with this problem, unless extremely large areas and number of pixels are considered.

Moreover, we have essentially limited our considerations to zero-width models for the transition regions between equipotential or constant magnetization stripes. However, it should be pointed out that the extension to more realistic models can be easily carried out by a suitable change of the Fourier coefficients. As in this case the inversion can be effected only numerically, it is possible to assess the reliability of the obtained results by comparing them to the those illustrated in this paper. As zero-width models represent the worst case, the errors introduced in their numerical inversion can be taken as an upper estimate of those made in the less extreme and more physical configurations. The same consideration holds for an estimate of the influence of the perturbed reference wave in a given holography set-up.

Last but not least, as shown by Mansuripur [14] and by our work on vortices in tilted specimens [1,2,4], the condition that the specimen is perpendicular to the electron beam is not essential and can be easily removed in the Fourier space approach.

Work is in progress where this approach is applied to other magnetic configurations and structures present in micro- and nano-particles [32].

## Acknowledgements

Useful discussions with Dr. R. Dunin-Borkowsky, Dr. P.G. Merli and Professor H. Lichte are gratefully acknowledged.

## References

- [1] M. Beleggia, G. Pozzi, *Ultramicroscopy* 84 (2000) 171.  
 [2] M. Beleggia, G. Pozzi, *Phys. Rev. B* 63 (2001) 54507.

- [3] R.G. Mints, V.G. Kogan, J.R. Clem, *Phys. Rev. B* 61 (2000) 1623.  
 [4] M. Beleggia, G. Pozzi, *J. Electron. Microsc. 51* (2002) S73.  
 [5] C. Capiluppi, P.G. Merli, G. Pozzi, in: *Institute of Physics (Ed.), Proceedings of the EMAG 75 Meeting, Developments in Electron Microscopy and Analysis*, Academic Press, London, 1976, pp. 233–236.  
 [6] C. Capiluppi, P.G. Merli, G. Pozzi, *Optik* 47 (1977) 205.  
 [7] P.G. Merli, G. Pozzi, *Optik* 51 (1978) 39.  
 [8] G. Pozzi, *Optik* 53 (1979) 381.  
 [9] M. Vanzi, *Optik* 68 (1984) 319.  
 [10] C. Capiluppi, A. Migliori, G. Pozzi, *Microsc. Microanal. Microstruct.* 6 (1995) 647.  
 [11] M. Beleggia, R. Capelli, G. Pozzi, *Philos. Mag. B* 80 (2000) 1071.  
 [12] M. Beleggia, P.F. Fazzini, G. Pozzi, *ICEM 2002 Conference Proceedings*.  
 [13] I.A. Beardsley, *IEEE Trans. Magn.* 25 (1989) 671.  
 [14] M. Mansuripur, *J. Appl. Phys.* 69 (1991) 2455.  
 [15] M. Mansuripur, *The Physical Principles of Magneto-optical Recording*, Cambridge University Press, Cambridge, 1995.  
 [16] G. Pozzi, *Adv. Imaging Electron. Phys.* 93 (1995) 173.  
 [17] G.F. Missiroli, G. Matteucci, G. Pozzi, *Adv. Imaging Electron. Phys.* 99 (1997) 171.  
 [18] G.F. Missiroli, G. Pozzi, U. Valdrè, *J. Phys. E: Sci. Instrum.* 14 (1981) 649.  
 [19] G.V. Spivak, G.V. Saporin, N.N. Sedov, L.F. Komolova, *Bull. Acad. Sci. USSR: Ser. Phys. (USA)* 32 (1968) 1046.  
 [20] A.H. Zemanian, *Distribution Theory and Transform Analysis: an Introduction to Generalized Functions with Applications*, McGraw-Hill, New York, 1965.  
 [21] M.J. Lighthill, *Fourier Analysis and Generalized Functions*, Cambridge University Press, Cambridge, 1970.  
 [22] D.S. Jones, *Generalized Functions*, McGraw-Hill, New York, 1966.  
 [23] I. Richards, H. Youn, *Theory of Distribution: a Non-technical Introduction*, Cambridge University Press, Cambridge, 1990.  
 [24] A.I. Saichev, W.A. Woyczyński, *Distributions in the Physical and Engineering Sciences*, Birkhäuser, Boston, 1997.  
 [25] E.O. Brigham, *Fast Fourier Transform and its Applications*, Prentice-Hall, Englewood Cliffs, NJ, 1997.  
 [26] R.N. Bracewell, *Two-dimensional Imaging*, Prentice-Hall, Englewood Cliffs, NJ, 1995.  
 [27] A.J. Jerri, *The Gibbs Phenomenon in Fourier Analysis, Splines and Wavelet Approximation*, Kluwer Academic Publishers, Dordrecht, 1998.  
 [28] M. Born, E. Wolf, *Principles of Optics*, Pergamon Press, Oxford, 1989.  
 [29] F. Gori, *Opt. Commun.* 48 (1983) 67.  
 [30] F. Gori, *Atti della Fondazione Giorgio Ronchi, Anno XXXVIII* 5–6 (1984) 593.  
 [31] I.S. Gradshteyn, I.M. Ryzhik, *Tables of Integrals, Series and Products*, Academic Press Inc., New York, 1980.  
 [32] M. Beleggia, Y. Zhu, *Philos. Mag. B*, in press.